Spectrochimica Acta Part A: Molecular and Biomolecular Spectroscopy 279 (2022) 121495

Contents lists available at ScienceDirect

Spectrochimica Acta Part A:
Molecular and Biomolecular Spectroscopy

journal homepage: www.journals.elsevier.com/spectrochimica-acta-part-a-molecular-and-biomolecular-spectroscopy

Apocynin reduces cytotoxic effects of monosodium glutamate in the brain: A spectroscopic, oxidative load, and machine learning study

Joanna Depciuch [a,1,*], Paweł Jakubczyk [b], Wiesław Paja [c], Jaromir Sarzyński [c], Krzysztof Pancerz [d], Merve Açıkel Elmas [e], Elif Keskinöz [f], Özlem Bingöl Özakpınar [g], Serap Arbak [e], Gökçe Özgün [h], Sevde Altuntaş [i,j], Zozan Guleken [k,1,*]

[a] Institute of Nuclear Physics Polish Academy of Science, 31–342 Krakow, Poland
[b] Institute of Physics, University of Rzeszów, Poland
[c] Institute of Computer Science, University of Rzeszów, Poland
[d] Institute of Technology and Computer Science, Academy of Zamosc, Poland
[e] Department of Histology and Embryology, Acibadem Mehmet Ali Aydinlar University, School of Medicine, Istanbul, Turkey
[f] Department of Anatomy, Acibadem Mehmet Ali Aydinlar University, School of Medicine, Istanbul, Turkey
[g] Department of Biochemistry, Marmara University Faculty of Pharmacy, Istanbul, Turkey
[h] Department of Medical Biotechnology, Health Sciences Institute, Acibadem Mehmet Ali Aydinlar University, School of Medicine, Istanbul, Turkey
[i] Tissue Engineering Department, University of Health Sciences Turkey, Istanbul 34662, Turkey
[j] Experimental Medicine Research and Application Center, Validebag Research Park, University of Health Sciences, Istanbul 34662, Turkey
[k] Department of Physiology, Uskudar University, Faculty of Medicine, Istanbul, Turkey

ARTICLE INFO

Keywords:
Monosodium glutamate
Apocynin
Brain tissue
Oxidative load
FTIR
Machine learning

ABSTRACT

Herein, we examined the modulatory effects of Apocynum (APO) on Monosodium Glutamate **(**MSG)-induced oxidative damage on the brain tissue of rats **after** long-term consumption **of** blood serum components by biochemical assays, Fourier transform infrared spectroscopy (FTIR), and machine learning methods. Sprague-Dawley male rats were randomly divided into the Control, Control + APO, MSG, and MSG + APO groups (n = 8 per group). All administrations were made by oral gavage saline, MSG, or APO and they were repeated for 28 days of the experiments. Brain tissue and blood serum samples were collected and analyzed for **measurement** levels of malondialdehyde (MDA), glutathione (GSH), myeloperoxidase (MPO), superoxide dismutase (SOD) activity, and Spectroscopic analysis. After 29 days, the results were evaluated using machine learning (ML). The levels of MDA and MPO showed changes in the MSG and MSG + APO groups, respectively. Changes in the proteins and lipids were observed in the FTIR spectra of the MSG groups. Additionally, APO in these animals improved the FTIR spectra to be similar to those in the Control group. The accuracy of the FTIR results calculated by ML was 100%. The findings of this study demonstrate that Apocynin treatment protects against MSG-induced oxidative damage by inhibiting reactive oxygen species and upregulating antioxidant capacity, indicating its potential in alleviating the toxic effects of MSG.

Abbreviations: APO, Apocynin; ATR, Attenuated total reflection; DNN, Deep Neural Networks; DTNB, 5,5′-dithiobis-2-nitrobenzoic acid; FTIR, Fourier transform infrared spectroscopy; GLU, Glutamic acid; GSH, Glutathione; INT, 2-(4-iodophenyl)-3-(4-nitrophenol)-5-phenyltetrazolium chloride; kNN, k-Nearest Neighbors; LOOCV, Leave-One-Out Cross Validation; MCC, Matthews correlation coefficient; MCT, Liquid-nitrogen cooled mercury cadmium telluride detector; MDA, Malondialdehyde; MPO, Myeloperoxidase; MSG, Monosodium Glutamate; NADH, Nicotinamide adenine dinucleotide; NADPH, Nicotinamide adenine dinucleotide phosphate; PCA, Principal Component Analysis; RF, Random forest; ROS, Reactive oxygen species; SD, Standard deviation of means; SOD, Superoxide dismutase; SVM, Support Vector Machine; TBA, Thiobarbituric acid; TCA, Trichloroacetic acid; TNB, 5-thio-2-nitrobenzoic acid.

* Corresponding authors at: Institute of Nuclear Physics Polish Academy of Science, 31-342 Krakow, Poland (J. Depciuch), Department of Physiology Uskudar University Faculty of Medicine, Saray site yolu Street, 34768 No/27, 34768 Ümraniye/İstanbul (Z. Guleken).
E-mail addresses: joanna.depciuch@ifj.edu.pl (J. Depciuch), zozan.guleken@uskudar.edu.tr (Z. Guleken).
[1] Equal senior author.

https://doi.org/10.1016/j.saa.2022.121495
Received 19 March 2022; Received in revised form 2 June 2022; Accepted 7 June 2022
Available online 9 June 2022

1. Introduction

Monosodium glutamate (MSG, the sodium salt of glutamic acid [GLU]), is a widely used flavor enhancer derived from naturally occurring L-glutamic acid in various food products [1]. The effects of MSG on brain tissue are still controversial and under investigation. Recent animal studies provide proof of its effects. Animal studies **have shown** that MSG administration, depending on the dose may cause degeneration in the brain, especially in the portions of the hypothalamus, which controls the secretion of several pituitary hormones, but researchers report that the most notable effects occur in the adulthood of the animals; animals were found under normal body length, obese, and have difficulty in reproductive functions [2]. Following this study, the authors proposed that feeding infants normal food containing MSG might also cause hypothalamic lesions [3]. Food-related neurotoxicity depends on the hypothesis that MSG consumption would cause plasma GLU levels to rise by increased GLU absorption by the intestine and entering the bloodstream. When enough MSG is consumed, the plasma GLU levels would rise high enough to elevate pituitary GLU levels. Small and large molecules from **the** blood freely enter the circumventricular organs 'areas in the brain since there is no blood–brain barrier. GLU results in **the** depolarization of neurons, as it is an excitatory neurotransmitter [4]. Overstimulated neurons die when exposed to too much GLU [5]. Glutamate release from activated microglia requires oxidative burst and lipid peroxidation [6], as shown in previous studies [7,8]. Apocynin has numerous anti-inflammatory effects, including decreasing neutrophil oxidative burst and neutrophil-mediated oxidative damage [9] reducing the adhesion of monocytic cells to human umbilical vein endothelial cells, treatment **by** tumor necrosis factor (TNF) [10], inhibiting polymorphonuclear granulocyte chemotaxis [11] inhibiting peroxynitrite [12] and inhibiting **the** destruction of cartilage mediated **by** inflammation [11]. Apocynum (APO), which can be obtained from the roots of the plant Apocynum cannabinum, has a NOX inhibitory effect and is an effective nicotinamide adenine dinucleotide (NADH) oxidase complex inhibitor [13,10]. Nicotinamide adenine dinucleotide phosphate (NADPH) oxidases (NOX) are relevant sources of reactive oxygen species (ROS) during excitotoxic damage. NADPH oxidase-2 (NOX-2) has been particularly related to neuronal damage and death, as well as to the resolution of the subsequent inflammatory response. This oxidative damage also has effects on biomacromolecules in blood and serum. Reactive oxygen species formed because of the increase in oxidative stress attack the double bond containing groups of intracellular lipid and protein structures and the double bonds of the bases in DNA and initiate chain oxidation reactions by breaking a hydrogen atom. As a result, macromolecules such as intracellular lipid, protein, and DNA are damaged, resulting in cell injury or cell death. To demonstrate these changes in detail, we performed FTIR spectroscopic measurements, which have been used in many studies [14,15,16,17].

However, FTIR spectroscopy provides global information about the chemical structure of the measured sample (e.g. tissue, serum, blood) [18]. Continuing, investigation of the content and structure of the protein or lipid fraction, but without prior functionalization. Consequently, it is not possible to indicate exactly in which for example protein, the visible in the FTIR spectra changes occurred. Moreover, the biological material is a complex structure, and some functional group vibrations can be attributed to two or more fractions. Therefore, advanced statistical and computational methods are needed that will unambiguously indicate the sensitivity of the method [19]. Consequently, spectroscopic data is used for calculations using multivariate analysis or machine learning methods [20]. Thanks to these methods, it is possible to clearly indicate the values of wavenumbers that are characteristic of a disease or changes caused by drugs or chemicals [18]. Therefore, this study aimed to investigate the neuroprotective effects of APO treatment induced by MSG on brain and blood serum using biochemical assays, spectroscopic measurements, and machine learning methods. For this purpose, serum collected from rats divided into 4 groups was analyzed using FTIR spectroscopy combined with Principal Component Analysis (PCA) and machine learning, as well as marking the level of MDA, MPO, SOD and GSH.

2. Materials and methods

2.1. Animals, drugs and experimental design

Animals were purchased from, the *Animal Research Centre of the* University of Acıbadem, Istanbul, Turkey. We used 8 weeks old Sprague-Dawley male rats (n = 24, 250–300 g) in this study Animals' housing and handling conditions were the same as described previously [19]. The rats were kept in a laboratory environment (Acıbadem University Experimental Animals Laboratory) with a standard light/dark (12/12 h) cycle at **a** controlled room temperature **of** 22 ± 2 °C throughout the experiment. Thirty-two rats were randomly divided into 4 groups (n = 8, each group). All rats in the experimental group were given standard rat chow and tap water ad libitum. The rats in the control group were given distilled water by the gavage method for 28 days. To evaluate the effect of MSG on the brain, rats in the MSG group were given a solution of 120 mg/kg for 28 days by the gavage method [20]. The rats in the Control + APO group were given 25 mg/kg Apocynin solution for 5 days [21] in the last 5 days of the experiment. While MSG solution (120 mg/kg) continued to be given to the rats in the treatment (MSG + APO) group, 25 mg/kg of Apocynin solution was given by **the** gavage method for 5 days from the 25th day of the experiment. MSG solution was prepared by diluting with physiological saline and given to rats. Apocynin solution was dissolved in DMSO and given to **the** rats. In this study, 4 experimental groups were formed, as shown in Table 1. All animal handling and experimentation were approved by the institutional ethics and animal care committee of the University of Acıbadem (ACU HADYEK 2022/18) and were conducted according to the guidelines of the National Institutes of Health Guide for the Care and Use of Laboratory Animals [22]. Monosodium glutamate (MSG; G1626, Sigma Aldrich, MA U.S.A.), Apocynin (APO; sc-203321, Santa Cruz, California, U.S.A.), 5,59-dithiol-bis (2-nitro benzoic acid) (DTNB), Trichloroacetic acid (TCA), Thiobarbituric acid (TBA), and Bovine serum albumin (BSA) were purchased from Sigma Aldrich (USA).

2.2. Measurements of oxidative load (oxidant/antioxidant)

2.2.1. Estimation of lipid peroxidation products

The extent of lipid peroxidation was measured by the estimation of malondialdehyde (MDA). **This method was** developed by Ohkawa et al. was used for the determination of tissue MDA, which is a marker of lipid peroxidation [23]. The principle of the method is based on measuring the color intensity of the pink complex formed by MDA, one of the degradation products of lipid peroxidation, with thiobarbituric acid (TBA) at a wavelength of 532 nm. Tissues removed immediately after decapitation were washed with physiological saline**,** dried with filter paper and weighed. Measurements were made by preparing 10% wt tissue homogenate with 150 mM KCl solution on ice with a homogenizer. The results were expressed as nmol/g protein.

Table 1
The experimental design.

	Administrations	Days
1-Control	Distilled water,120 mg/kg per day	0 to 28
2-Control + APO	Distilated water, 120 mg/kg per day; Apocynin, 25 mg/kg per day	0 to 23; 24 to 28
3-MSG	MSG, 120 mg/kg per day	0 to 28
4-MSG + APO	MSG, 120 mg/kg per day; Apocynin, 25 mg/kg	0 to 23; 24 to 28

2.2.2. Antioxidant enzyme activity

The activity of the antioxidant enzyme superoxide dismutase (SOD) determination in tissue was made according to the method of Sun et al. [24]. Tissue homogenate to be diluted with 10 mM phosphate buffer (pH 7.00), diluted homogenate 0.05 mmol/L in a buffer solution containing 50 mmol/LCAPS (3-(cyclohexylamine)-1-propane sulfonic acid) and 0.094 mmol/L EDTA (pH 10.2) xanthine sodium and a substrate solution containing 0.025 mmol/L 2-(4-iodophenyl)-3-(4-nitrophenol)-5-phenyltetrazolium chloride (INT). The increase in absorbance, which was measured for 532 nm wavelength, was observed by adding xanthine oxidase (80 U/ml) to the mixture.

2.2.3. Estimation of GSH

GSH determination in **tissues was** determined according to the method of Beutler et al. (Beutler, Duron, et al. 1963) [25]. In the determination of glutathione, 10% homogenates prepared for MDA determination were used. 0.4 ml of 10% homogenate and 0.2 ml of 20% Trichloroacetic acid (TCA) were mixed and centrifuged at 3000 rpm for 15 min and GSH was studied in the upper phase. The sulfhydryl group of GSH reacts with 5,5′-dithiobis-2-nitrobenzoic acid (DTNB, Ellman's reagent) to form yellow 5-thio-2-nitrobenzoic acid (TNB). The GSH concentration was determined by measuring the absorbance of this colored product at 412 nm wavelength.

2.2.4. Estimation of MPO

The tissue MPO activity was performed using a commercially purchased kit. Standard solutions prepared as specified in the kit procedure were added as 50 μl to the antibody-coated 96-well plate. Again, 40 μl of the sample diluent solution, which was ready in the kit, was added to the wells. 10 μl of tissue samples were taken, and the volume of the sample wells was made up to 50 μl and incubated at 37 °C for 30 min. After incubation, the plate was washed 5 times with the wash solution. Then, 50 μl of HRP-Conjugate reagent was added to each well and incubated again at 37 °C for 30 min. After incubation, the rewashing stage was carried out. Equal concentrations of chromogen solutions were added to the wells and incubated at 37 °C for 15 min in the dark. At the end of the period, the stop solution was added and the plate was measured using a spectrophotometer at 450 nm wavelength.

2.2.5. Estimation of Albumin

Albumin levels were measured using the "Teco Diagnostics- Albumin Reagent Set." Samples were prepared in and mixed with vortex and maintained at room temperature for 5 min. After the dwell time, the tubes were read at 630 nm against the blank. Results are given in g/dL.

2.2.6. FTIR system setup

In this study, we used an FTIR spectrometer device (Nicolet İS50 FT-IR, Thermo Fischer Scientific, Waltham, Massachusetts, USA), equipped with **an** attenuated total reflection (ATR) accessory and licensed at the University of Health Sciences, Validebağ Research Park. The sample detection was made with liquid-nitrogen cooled mercury cadmium telluride (MCT) detector.

The serum samples were naturally thawed before the measurement. ATR crystal plate was washed with 70% ethanol and dried with **a** soft paper before use and between measurements of each sample. Before the measurements, the background absorption spectrum. Subsequently, 4 μl samples were dropped onto an ATR crystal plate using a pipette. After drying at room temperature for 5 min, FTIR measurements **were** performed as described previously [16]. All samples were measured in the range between 400 cm^{-1} and 4000 cm^{-1} using 64 scans with 8 cm^{-1} spectral resolution. The spectra were recorded with OMNIC software (Thermo Fisher Scientific, Waltham, USA), however, baseline correction and vector normalization were performed using OPUS software (Bruker, Germany).

2.2.7. Data processing and analysis

This study was conducted using the GraphPad Prism 6.1.0 program (GraphPad Software, San Diego, CA, USA). A one-way ANOVA was performed followed by a posthoc Tukey test. All data are expressed as mean ± standard deviation of means (SD). A significant difference was noted as $*p < 0.05$.

2.2.8. Analyses of FTIR data using Principal Component Analysis, differences in the absorbance dynamics, and machine learning

To show differences in the chemical compounds in serum collected from animals, the second derivative of FTIR spectra **was** calculated using 9 smoothing points in OPUS software. In the obtained spectra, differences in the peak position were analyzed. Furthermore, to obtain information about differentiate samples from other groups, Principal Component Analysis (PCA) was performed using Past 3.0 software in the FTIR range between 800 cm^{-1} and 1800 cm^{-1}. For this purpose, 1038 data points for each sample were analyzed to obtain the most variance components significant. PCA was performed to investigate if the obtained chemical changes caused by MSG, MSG treatment with APO, as well as only APO in the control group, which was visible in the FTIR spectra were significant. Moreover, PCA showed, if the chemical changes were significant and caused, that the analyzed groups differed from each other.

The absorption dynamics method is based on the fact that light is absorbed in a sample, which corresponds to the vibrational frequencies of the bonds in the sample. As a result, one obtains a spectrum i.e. absorption as a function of wavenumbers. It is supposed that such a spectrum may be altered due to tissue disease or taking medication and is generally different from the spectrum of healthy tissue. To distinguish diseased tissue from healthy tissue, we use here a comparative method based on comparing the dynamics of the spectra of both tissues for all wave numbers. Such an approach allows to find wavenumbers that simultaneously mark different dynamics for diseased tissue, therefore these wavenumbers can be considered potential markers to discriminate diseased tissue only by their FTIR spectrum. We developed computer procedures to calculate the differences in dynamics for two different groups of samples, which allowed us to determine the wavenumbers where these differences are significant. Here, to find the differences in the FTIR spectrum between the Control and MSG, as well as MSG and MSG + APO groups, differences in the absorbance dynamics, were calculated. The calculations were performed in a Matlab Simulink environment (MathWorks, Natick, MA).

To assess the quality of the classification accuracy among Control to MSG, and MSG to MSG + APO animals computational experiments were conducted. Additionally to mathematically describe the accuracy of a test, which reports the presence or absence of a condition The sensitivity, and specificity were calculated to validate methods. Sensitivity allows for determining the percentage of individuals who test positive for a condition that has that condition. On the other hand, the specificity parameter is the percentage of individuals without the condition who test negative for that condition. A set of parameters including Matthews correlation coefficient (MCC) [26] which is used as a measure of the quality of binary (two-class) classifications and additionally F1 score [27] which is a measure of a test's accuracy were also calculated. We applied six machine learning methods: Random forest (RF) [28], C5.0 decision tree algorithm [29], k-Nearest Neighbors (kNN) with $k = 5$, [30], Deep Neural Networks (DNN) [31], Support Vector Machine (SVM), [32], and XGBoost trees, [33]. The machine learning algorithms used were chosen to be a representation of methodologically different approaches to building learning models.

DNN is based on artificial neuron networks. They consist of multiple layers to progressively extract higher-level features from the input data set. As a deep learning model to classify data, we have used the neural network with the following consecutively connected layers:

- a dense layer with 4nda neurons,

- a dense layer with 2nda neurons,
- a dense layer with nda neurons,
- a dense layer with 1 neuron

where n_{da} is the number of features in the input data set. The dependence of the number of neurons in each layer is dictated by the desire to establish fair conditions for assessing the accuracy of classification. It is worth noting that the input data sets have a significantly different number of features, especially after their selection. The SVM classifier constructs a set of hyperplanes that are used for classification. The XGBoost classifier is a decision tree-based machine learning algorithm that uses gradient boosting. Generally, boosting is an ensemble *meta*-algorithm that converts weak models (typically decision trees) to strong ones. In the experiments, we set the maximum depth of trees equal to 4. Random forest is an ensemble classifier algorithm where individual classifiers are binary decision trees. A default parameter of 500 trees was used in the experiments. The C5.0 algorithm, on the other hand, is a traditional single decision tree algorithm based on an information gain parameter. The kNN algorithm, on the other hand, is a supervised data clustering method where the classification is based on placing an object in a multidimensional case space and classifying it based on the category that its nearest neighbors have. The number of 5 neighbors was used in the experiments.

To calculate the mentioned classification quality assessment parameters, the raw data obtained from the spectroscopy experiments were formatted into decision tables. This was necessary to prepare the input data for the ML algorithms used. Such a table consists of columns containing absorption values for particular wavenumbers and rows containing absorption values for individuals. The last column, the so-called decision column, contains the name of the individual category: control group, Control + APO, MSG, or MSG + APO. For the FTIR experiments, the number of columns is 1038 (the number of waves). An excerpt from the sample decision table is shown in Table 2.Table 3.

For each category, the number of individuals/learning cases was seven. Calculations were performed in the R environment using selected computational packages: class, caret, randomForest, C5.0, keras, xgboost, and e1071. Additionally, during testing, the Leave-One-Out Cross-Validation (LOOCV) method was applied. This method is appropriate when we have a small dataset or when an accurate estimate of model performance is more important than the computational cost of the method. LOOCV is a case of Cross-Validation where just a single observation is held out for validation. The model was evaluated for every hold - out observation. The final result is then calculated by taking the mean of all individual evaluations. Additionally, in the second part of the experiments, we used the Boruta relevant feature selection method [36] to identify relevant features (wavenumbers) from the original set of features and to create a subset of relevant features.

3. Results

3.1. Biochemical changes in brain tissue

As shown in Fig. 1, MPO level was measured to estimate the oxidative stress in groups of brain tissue. Compared to the Control group, MPO level (38.9 ± 14.8 mg) was significantly decreased compared to Control + APO (70.3 ± 12.3 mg; $p < 0.001$), MSG (91.5 ± 10.4 mg; $p < 0.001$), and MSG + APO (64.7 ± 12.5 mg; $p < 0.01$) groups with mean ± SD as seen in Fig. 1a. In the case of MDA level, which was measured for **estimating** the lipid peroxidation product, compared **with** the Control group (5.28 ± 2.22 nmol/g) MDA level was decreased in the Control + APO (3.52 ± 1.89 nmol/g; $p < 0.05$*)* group, elevated in the MSG group (15.36 ± 6.47 nmol/g; $p < 0.01$) and MSG + APO group (7.03 ± 3.73 nmol/g). Also, there was a significant MDA in the crease in the MSG group compared to the Control + APO group ($P < 0.01$) as seen in Fig. 1b. SOD level was decreased in the Control + APO (99.5 ± 6.23 IU/g) group and MSG group (86.3 ± 9.86 IU/g; $p < 0.05$) compared to the Control group (102.9 ± 18.99 IU/g). SOD level was increased in the MSG + APO group (107.3 ± 3.25 IU/g) compared to the control group as shown in Fig. 1c Furthermore, GSH levels were increased in the Control + APO group (14.30 ± 4.232 IU/g) MSG group (5.81 ± 0.587 IU/g; $p < 0.001$) and MSG + APO group (2.78 ± 8.024 IU/g; $p < 0.001$) compared to the Control group (18.57 ± 4.866 IU/g). Also, compared to the Control + APO groups, there was a significant decrease **in both the** MSG ($p < 0.01$) and MSG + APO groups ($p < 0.01$) as presented in Fig. 1d.

Albumin levels were decreased in the Control + APO group (4.27 ± 0.491 g/dL), MSG group (3.53 ± 0.487 g/dL; $p < 0.01$) and MSG + APO group (3.79 ± 0.395 g/dL) compared to the Control group (4.48 ± 0.384 g/dL). Also, compared to the Control + APO group, there was a significant decrease in the MSG group too ($p < 0.05$), Fig. 2.

Table 3
Regions of wavenumbers can be used as potential markers to discriminate MSG and MSG + APO animals by IR spectrum.

IR regions distinguish MSG and Control groups (wavenumbers, cm^{-1})	IR regions distinguish MSG and MSG + APO groups (wavenumbers, cm^{-1})
889–891	821–824
973–975	909–913
1177–1181	1008–1011
1199–1202	1365–1367
1295–1297	1388–1390
	1508–1512
	1666–1670
	1794–1796

3.2. Spectroscopic analysis along with PCA, changes in the absorbance dynamics, and machine learning methods

Protein and lipid structures in the analyzed groups of rats were obtained using the second derivative of **the** FTIR range corresponding to amide III (1250 cm^{-1}–1350 cm^{-1}), amide II (1470 cm^{-1}–1570 cm^{-1}) and amide I (1600 cm^{-1}–1700 cm^{-1}) [34], Fig. 3a, b, c, respectively, **and** lipids vibrations (2750 cm^{-1}–3050 cm^{-1}) [35], Fig. 3d, were analyzed.

In Fig. 3a, shifts of peaks at 1303 cm^{-1} and 1338 cm^{-1} toward lower wavenumbers, and peaks at 1315 cm^{-1} toward higher numbers were observed in the MSG group in Comparison with Control one. Administration of APO in the MSG + APO group caused lower changes in the peak positions than in animals without APO. In the amide II FTIR range, the shift of peaks at 1520 cm^{-1} and 1540 cm^{-1}, as well as 1560 cm-1, **were** visible in the MSG + APO group compared with Control one, Fig. 3b. The first peak shifted toward higher wavenumbers and the two next peaks toward lower wavenumbers. Also, in this case, the addition of APO caused decreased differences in the peak position between MSG + APO and Control groups. In the FTIR range originating from amide, I vibration, the shift of peaks at 1651 cm^{-1} and 1670 cm^{-1} corresponding

Table 2
A method of transforming spectral data to ML analysis.

1800.25308	1799.28883	1798.32458	…	801.2911	800.32685	Class
0.04314	0.04318	0.04302	…	0.04847	0.04903	MSC
0.04177	0.04156	0.04132	…	0.03611	0.03612	MSC
…	…	…	…	…	…	…

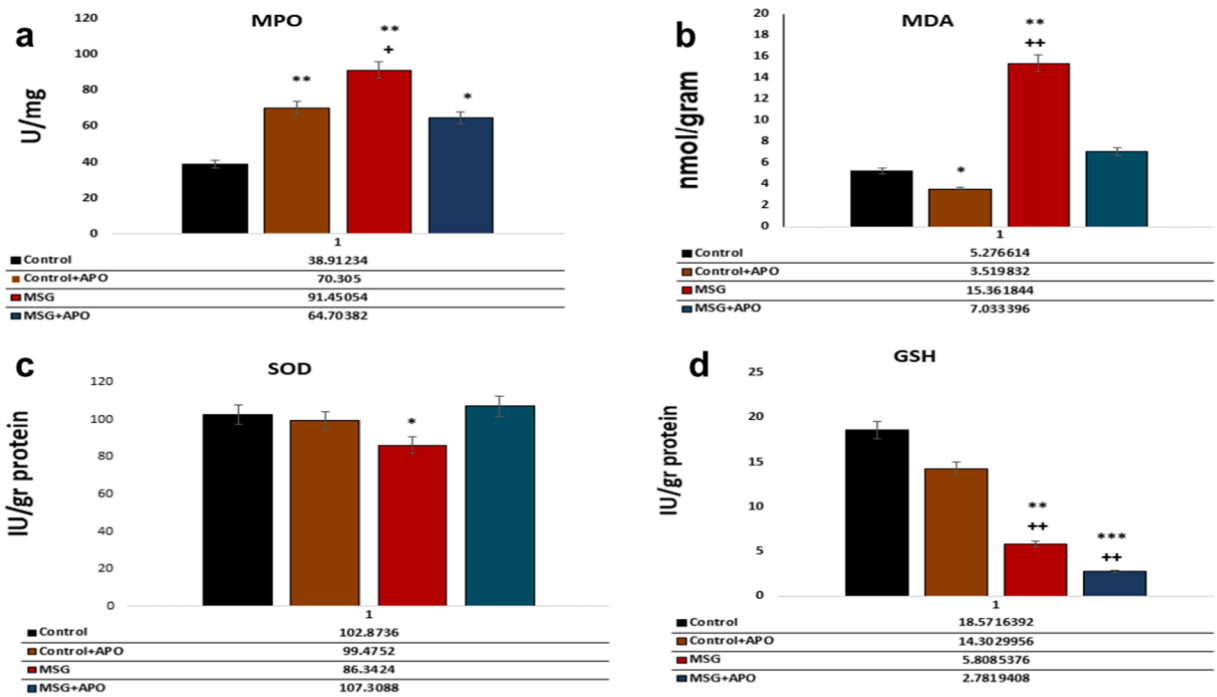

Fig. 1. Comparison of the oxidative stress-related index analysis (including MDA, MPO, SOD, and GSH) in rats from each group. Note: *P < 0.05 compared with the Control group; +P < 0.05 compared with the Control + APO group brain tissue.

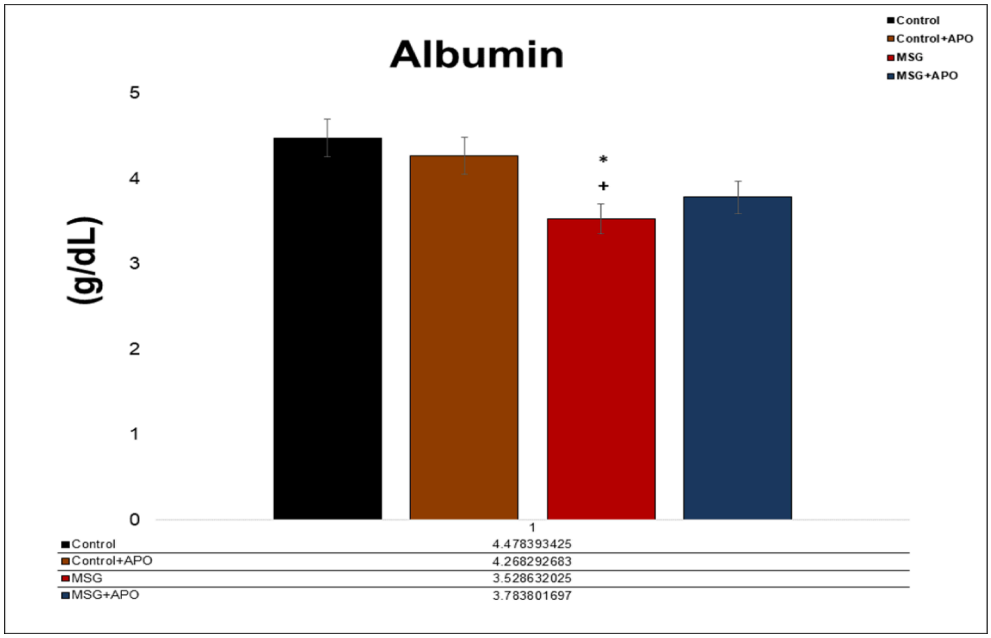

Fig. 2. Albumin levels of groups.

to α-helical, to lower wavenumbers and peaks at 1680 cm^{-1} and 1697 cm^{-1} originating from β-harmonica [36,37,38], **to** higher wavenumbers in the MSG + APO group compared with the Control group was noticed. FTIR spectra of MSG + APO animals showed, that the changes in the place positions were smaller and more similar to the control group than with the MSG group. Finally, changes in the peak position and spectrum structure of CH_2 and CH_3 lipid vibrations [39] were visible in FTIR spectra of MSG and MSG + APO compared with the control group. Importantly, in this case, APO did not correct the changes in the structure of the FTIR spectrum of MSG-APO animals, Fig. 3d.

To show the importance of biochemical changes caused by monosodium glutamate and the protective effect of APO, PCA was performed, **to show** whether the groups being studied could be distinguished, Fig. 4. Consequently, this analysis showed whether the biochemical changes are so significant that the groups differ statistically from each other.

PCA analysis showed, that using components PC1 (44.7%) and PC2 (22.2%), the samples collected from MSG + APO and Control, as well as MSG and Control were placed partially in the same quadrant of the coordinate system, Fig. 4a. However, analysis of PC1(44.7%) and PC3 (9.6%) showed, that MSG, MSG + APO, Control, and Control + APO can be distinguished from each other because all samples were collected

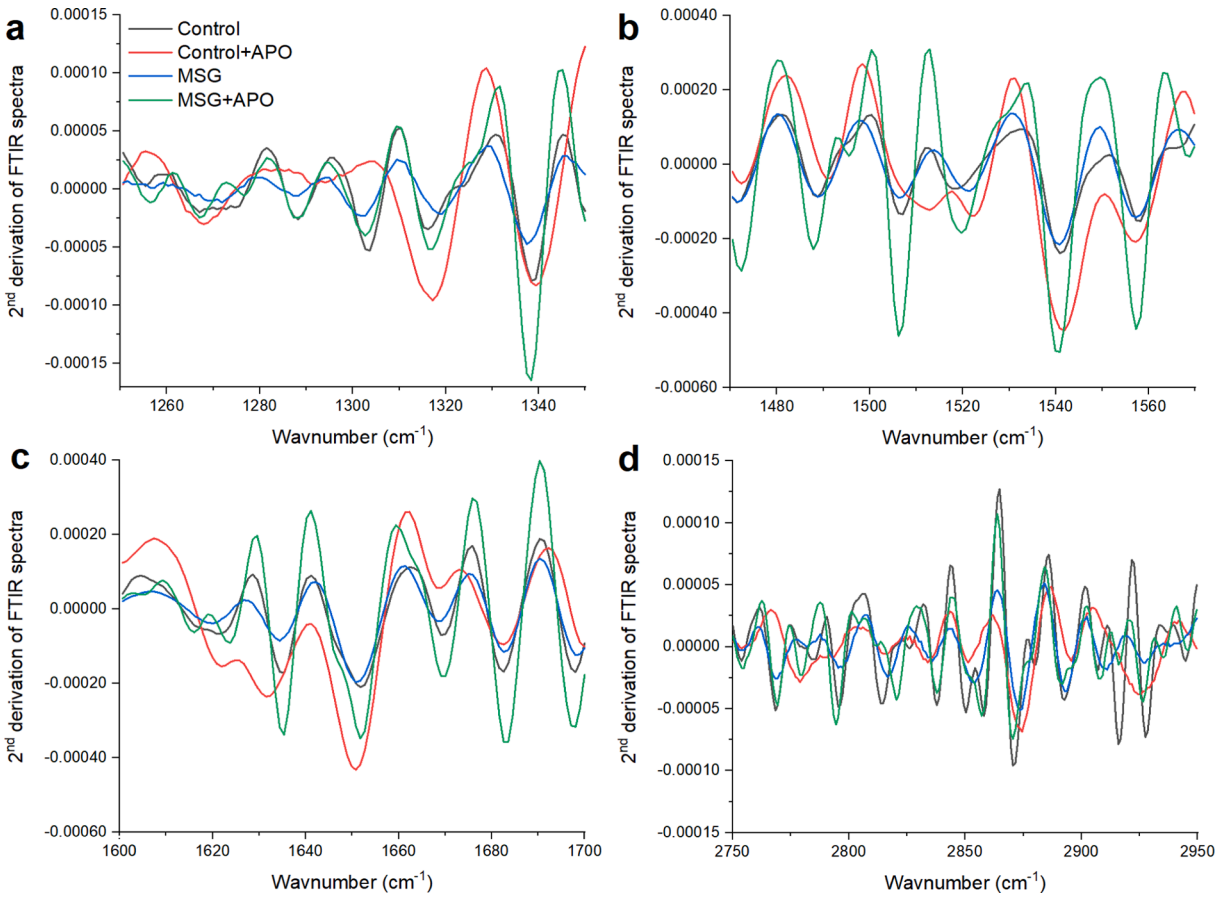

Fig. 3. Average second derivative of serum FTIR spectra in the range between the following: 1250 cm^{-1} and 1350 cm^{-1} (a); 1470 cm^{-1} and 1570 cm^{-1} (b); 1600 cm^{-1}–1700 cm^{-1} (c) and 2750 cm^{-1}–2950 cm^{-1} (d). Serum being studied was collected from animal groups: Control (black line), Control + APO (red line), MSG (blue line) and MSG + APO (green line).

from the same group were located in the other quadrant of the coordinate system, Fig. 4b. Samples from the Control group were placed in the positive value of PC1 and PC3, while FTIR spectra of serum collected from Control + APO characterized negative values of both components. Samples of the MSG group showed a negative value of PC1 and a positive value of PC3, while samples of MSG + APO **had a** positive value of C1 and a negative value of PC3. **The loading** plots of components, Fig. 4b, c, and d showed, that it is difficult to present, which wavenumbers were characteristic for each analyzed group, therefore dynamics in the absorbance of FTIR spectra, were performed, Fig. 5.

Based on the results presented in Fig. 5a and b one can distinguish regions of wavenumbers, which simultaneously marked different dynamics between **the** MSG and Control groups, as well as between MSG + APO and MSG groups. These wavenumbers regions were presented in Table 1. Therefore, these regions can be used as potential markers to discriminate MSG and MSG + APO only by their IR spectrum.

From Table 2, it can be noted, that MSG caused the most visible and significant changes in the amide III region and phospholipids. Furthermore, it was also visible, that **the** addition of APO caused changes in the three amides, which were also observed in the second derivative of the FTIR spectra presented in Fig. 3.

Computational experiments were conducted comparing the selected categories in pairs: MSG and Control as well as MSG + APO and MSG. The results of the parameters for assessing the accuracy of classification and identification of Control and MSG groups in the range between 1800 cm^{-1} and 800 cm^{-1} and selected wavenumbers are presented in Fig. 6. Additionally, a comparison of the ranges of absorption values with the individual wavelength importance values obtained from the feature selection algorithm is presented in Fig. 7.

Fig. 6 shows that the accuracy of the FTIR data is between 87% and 100%, depending on the usage of the machine learning methods. In five cases, **the** accuracy was 100%, and only the C5.0 method gave 87% accuracy. Moreover, this tendency was visible for the fingerprint FTIR region (1800 cm^{-1}–800 cm^{-1}) as well as for selected data.

Fig. 7 shows, that the most relevant FTIR wavenumbers, which could be used to distinguish MSG and Control groups were between 800 cm^{-1} and 1510 cm^{-1}, 1559 cm^{-1} and 1630 cm^{-1}, and between 1655 cm^{-1} and 1800 cm^{-1}. These results were confirmed **by** the data presented in Fig. 5.

Furthermore, the results of the parameters for assessing the quality of classification and identification of MSG and MSG + APO groups in the range between 1800 cm^{-1} and 800 cm^{-1} and selected wavenumbers showed, that the accuracy was between 71% and 93% for the fingerprint FTIR region, and between 93% and 100% for selected 6 wavenumbers (Fig. 8), depending on the usage of the machine learning methods.

The MSG and MSG + APO groups showed the most relevant, important differences in the FTIR ranges between 1505 cm^{-1} and 1507 cm^{-1} and between 1539 cm^{-1} and 1541 cm^{-1}, Fig. 9. This means, that APO caused biochemical changes in the functional groups located at these wavenumbers.

From the results obtained using machine learning methods, it can be seen that the FTIR approaches used in the analysis of the wave absorption levels of individual pairs of categories are an effective method for identifying these categories. For pairs of Control and MSG, as well as MSG and MSG + APO the spaces of absorption values are mostly separable sets, hence it is easy to identify multiple wavelengths that uniquely identify each category. The results obtained confirm the effectiveness of the proposed methods. However, they require larger studies with more cases of individuals from each category.

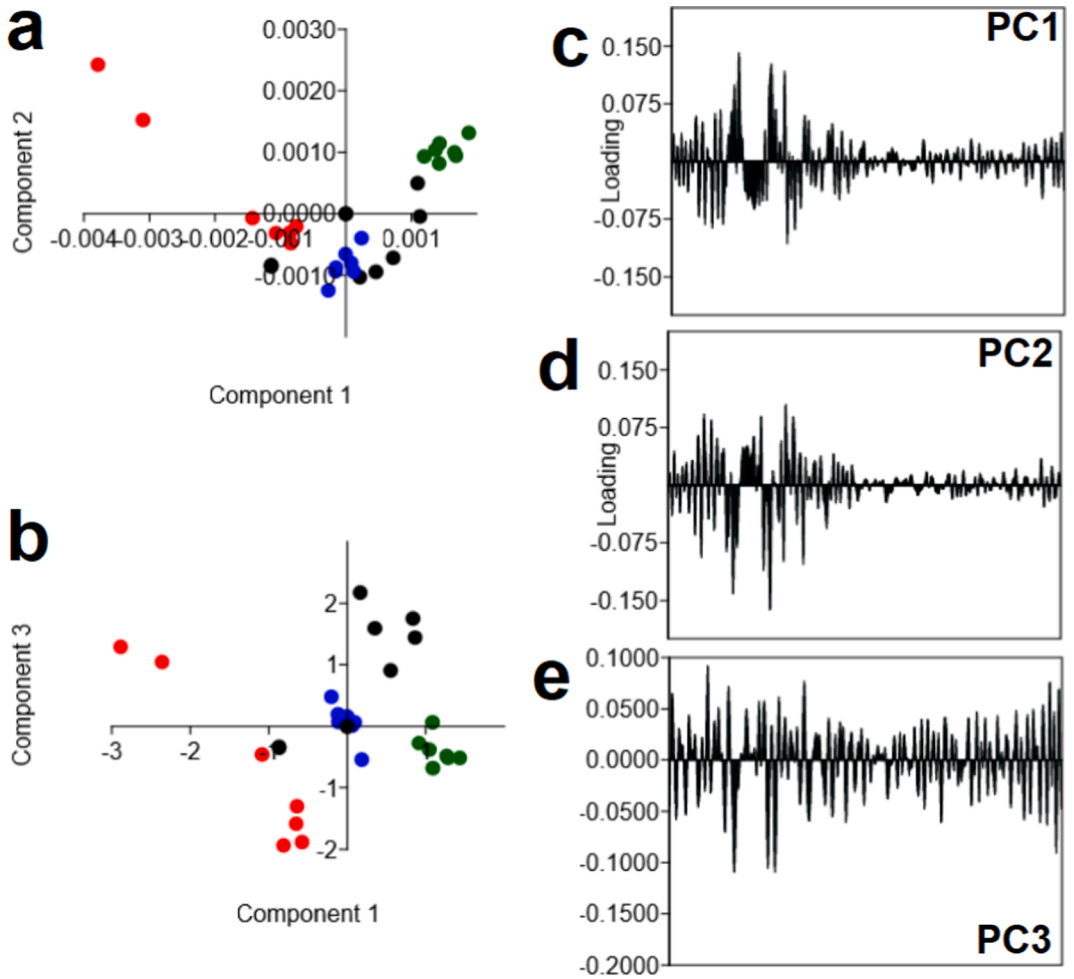

Fig. 4. PCA analysis of serum FTIR spectra in the range between 800 cm^{-1} and 1800 cm^{-1} (a, b) with PC1 (c), PC2 (d), and PC3 (e) loading plots, where serum being studied was collected from animals groups: Control (black dot), Control + APO (red dot), MSG (blue dot) and MSG + APO (green dot).

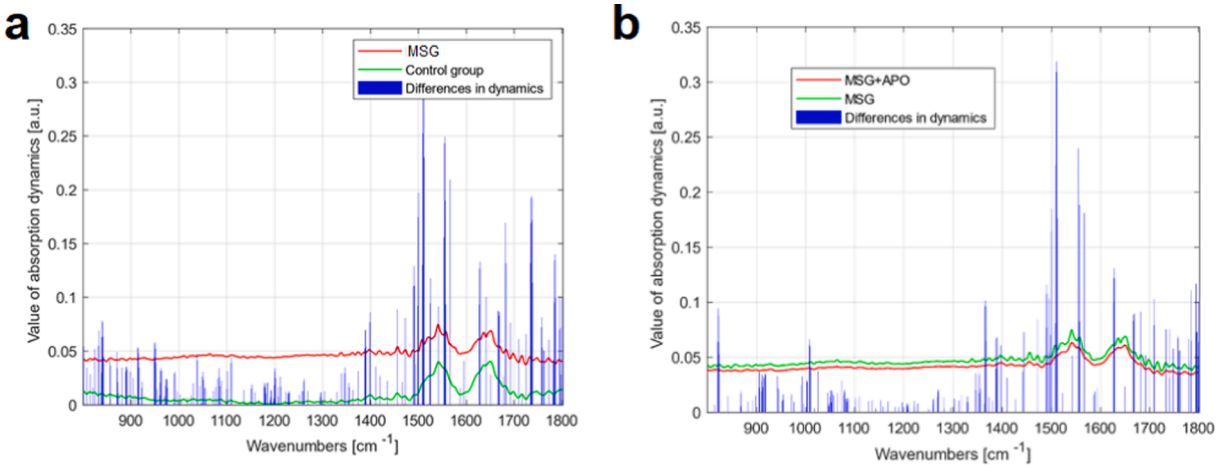

Fig. 5. Differences in the absorption dynamics of FTIR spectra between Control and MSG group (a) and between MSG + APO and MSG group (b).

4. Discussion

In this study, the cytotoxic effects of monosodium glutamate by apocynin were investigated. MSG acts on the glutamate receptors and consequently releases neurotransmitters, which play a critical role in normal physiological and pathological processes [40]. Glutamate receptors have three groups of metabotropic receptors, which are present across the central nervous system, particularly in the hypothalamus, hippocampus, and amygdala [41]. Additionally, MSG is one of the most widely used food additives in commercial foods, and results obtained from animal and human studies have shown, that the administration of even the lowest dose of MSG has toxic effects [42]. Therefore, it is crucial to find substances, which will reduce the negative impact of MSG on health. One of the proposed substances is apocynin, which is an

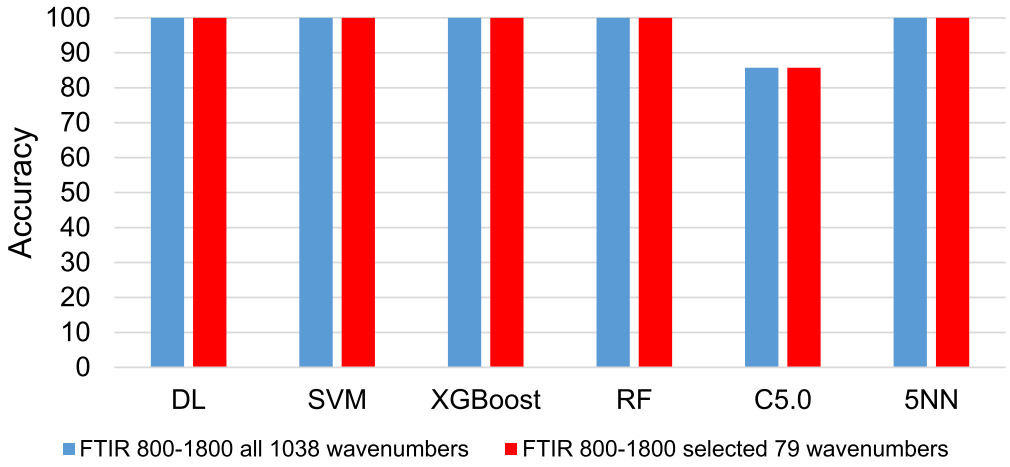

Fig. 6. Mean Accuracy values were obtained during the LOOCV analysis of Control and MSG data by the FTIR method considering the whole wavenumber range and the range of selected 79 relevant wavenumbers.

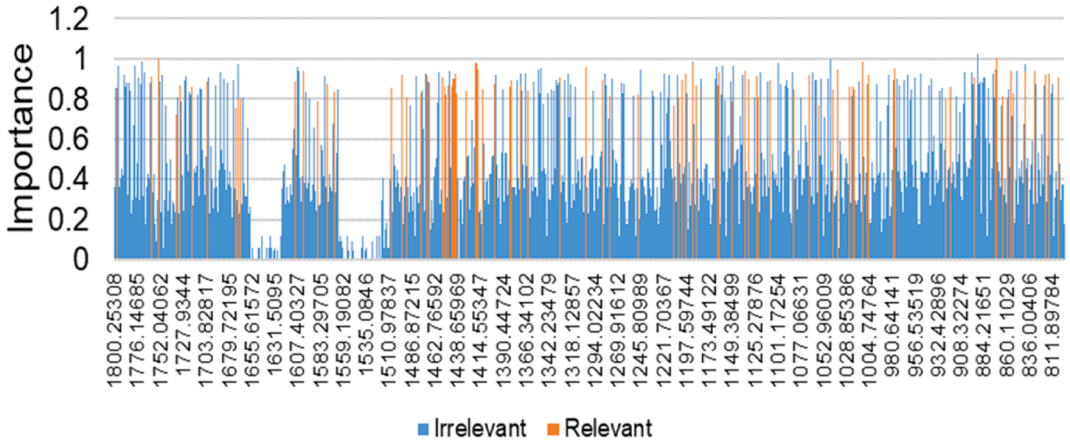

Fig. 7. Mean importance values of individual wavenumbers were obtained using the feature selection algorithm during the analysis of Control and MSG data.

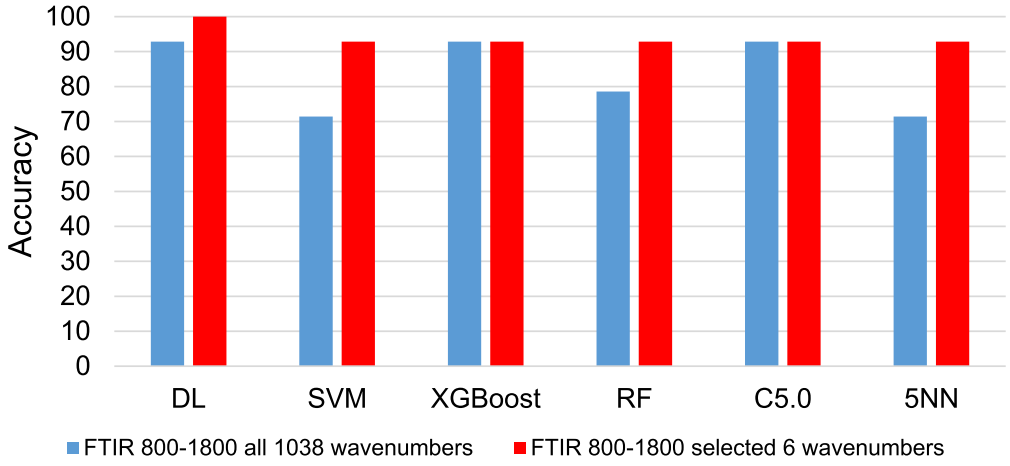

Fig. 8. Mean Accuracy values were obtained during the LOOCV analysis of MSG and MSG + APO data by the FTIR method considering the whole wavenumber range and the range of selected 6 relevant wavenumbers.

antioxidant compound [43] that cause**s** opposite changes in the human body as MSG. Our results **are shown** in Fig. 1 showed, that in animals administration by APO and foods with high levels of MSG, levels of MDA and MPO **are lower** than in animals without **the** addition **of** APO. These results suggest the antioxidant effect of APO. Importantly, in the case of MDA, the level is similar to that of the control group. Furthermore, the SOD level in the MSG + APO group was higher than in MSG and even in than in the control group, Fig. 1. Also, the albumin level in the MSG + APO group was higher than in MSG, Fig. 2. All of this suggests, that APO showed antioxidant properties [42]. Furthermore, analysis of changes in the dynamics absorption presented in Fig. 5b also showed, that APO can affect the amide vibrations, which build protein structure.

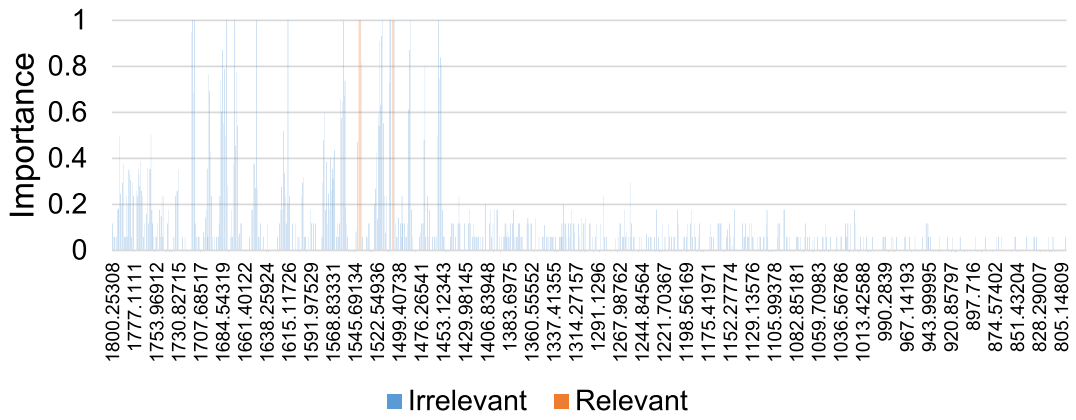

Fig. 9. Mean importance values of individual wavenumbers were obtained using the feature selection algorithm during the analysis of MSG and MSG + APO data.

Moreover, also spectroscopic analysis showed biochemical changes caused by MSG, Fig. 3. In the MSG second derivative of the FTIR region corresponding to amides III, II, and I, shifts of peaks toward lower and higher wavenumbers, were observed compared with the control group. Especially changes in the peak position in the amide I region showed structural changes in proteins, which were visible as changes in the α-helical and β-harmonica peak positions [34]. The protein changes visible in the FTIR spectra were correlated with changes in the albumin levels presented in Fig. 2. MSG can cause oxidative stress and directly and indirectly protein modification [44]. Consequently, differences in the amide structure can be caused by MSG. Interestingly, in the MSG + APO group, the shifts of peaks in **the** amide FTIR region were lower value, than in the MSG group, compared to **the** control one, Fig. 3a, b, c. It can be suggested, that apocynin **has** a preventive effect [45]. Also, in the FTIR region originating from lipid vibrations, changes in the structure of the spectrum and peak positions in the MSG group were visible compared with **the** control one, Fig. 3d. MSG very often causes lipid peroxidation [6] and consequently, this effect can be visible in the FTIR spectra. Furthermore, the structure of lipids FTIR region in the MSG + APO group was similar to the control group in the ranges between 2750 cm^{-1} and 2900 cm^{-1}, which can suggest a protective role of apocynin concerning monosodium glutamate [46]. PCA confirmed, that samples collected from MSG animals were not similar to control one, Fig. 4a, b. However, also samples collected from MSG-APO and Control + APO groups were placed in the other part of the coordinate system than **the** Control groups. Indeed, APO can cause biochemical changes such as increasing the concentration of antioxidant enzymes, having a preventive effect on lipids and affect**ing** the electrolyte balance [47]. These changes are very significant for the organism and consequently, **give** different spectroscopic characteristic**s**.

5. Conclusion

The findings of this study demonstrate for the first time that apocynin treatment provides neuroprotection against long-term MSG-induced oxidative damage. These observations were confirmed by biochemical assays and FTIR spectroscopy. Obtained results showed, that APO decreased MPO and MDA levels in the MSG + APO group compared with the MSG group. Furthermore, the increase in SOD level was visible in MSG rats administered APO. In FTIR spectra, changes in the amides III, II, and I **and** lipid vibrations were observed in the MSG + APO group compared with Control one. Interestingly these, changes were decreased with APO addition, and consequently, FTIR spectra of the MSG + APO group were more similar to controls than MSG animals. The accuracy in distinguishing biochemical changes by FTIR is 100%, which showed, then physical and computational methods can be used in a study on apocynin reducing cytotoxic effects of monosodium glutamate.

CRediT authorship contribution statement

Joanna Depciuch: Conceptualization, Methodology, Data curation, Formal analysis, Writing – original draft, Writing – review & editing, Visualization, Supervision. **Paweł Jakubczyk:** Conceptualization, Methodology, Data curation, Formal analysis, Writing – review & editing. **Wiesław Paja:** Formal analysis, Data curation, Writing – review & editing. **Jaromir Sarzyński:** Data curation, Formal analysis, Methodology, Data curation, Writing – original draft, Writing – review & editing. **Krzysztof Pancerz:** Methodology, Data curation, Formal analysis, Writing – original draft, Writing – review & editing. **Merve Açıkel Elmas:** Writing – review & editing. **Elif Keskinöz:** Writing – review & editing. **Özlem Bingöl Özakpınar:** Writing – review & editing. **Serap Arbak:** Conceptualization, Methodology, Writing – review & editing. **Gökçe Özgün:** Writing – review & editing. **Sevde Altuntaş:** Writing – review & editing. **Zozan Guleken:** Conceptualization, Methodology, Data curation, Formal analysis, Writing – original draft, Writing – review & editing, Visualization, Supervision.

Declaration of Competing Interest

The authors declare that they have no known competing financial interests or personal relationships that could have appeared to influence the work reported in this paper.

Acknowledgments

None

Data Sharing

Data will be made available upon request.

References

[1] A. Zanfirescu, A. Ungurianu, A.M. Tsatsakis, G.M. Nițulescu, D. Kouretas, A. Veskoukis, D. Tsoukalas, A.B. Engin, M. Aschner, D. Margină, A review of the alleged health hazards of monosodium glutamate, Compr. Rev. Food Sci. Food Saf. 18 (4) (2019) 1111–1134, https://doi.org/10.1111/1541-4337.12448.
[2] J.W. Olney, Brain lesions, obesity, and other disturbances in mice treated with monosodium glutamate, Science (80-) 164 (3880) (1969) 719–721.
[3] J.W. Olney, OI.-LAN. Ho, Brain damage in infant mice following oral intake of glutamate, aspartate or Cysteine, Nature 227 (5258) (1970) 609–611, https://doi.org/10.1038/227609b0.
[4] R.A. Hawkins, The blood-brain barrier and glutamate, Am. J. Clin. Nutr. 90 (3) (2009) 867S–874S, https://doi.org/10.3945/ajcn.2009.27462BB.
[5] B. Meldrum, J. Garthwaite, Excitatory amino acid neurotoxicity and neurodegenerative disease, Trends Pharmacol. Sci. 11 (9) (1990) 379–387, https://doi.org/10.1016/0165-6147(90)90184-A.
[6] S.W. Barger, M.E. Goodwin, M.M. Porter, M.L. Beggs, Glutamate release from activated microglia requires the oxidative burst and lipid peroxidation,

J. Neurochem. 101 (5) (2007) 1205–1213, https://doi.org/10.1111/j.1471-4159.2007.04487.x.
[7] V. Pavlovic, D. Pavlovic, G. Kocic, D. Sokolovic, T. Jevtovic-Stoimenov, S. Cekic, D. Velickovic, Effect of monosodium glutamate on oxidative stress and apoptosis in rat thymus, Mol. Cell. Biochem. 303 (1-2) (2007) 161–166, https://doi.org/10.1007/s11010-007-9469-7.
[8] E.O. Farombi, O.O. Onyema, Monosodium glutamate-induced oxidative damage and genotoxicity in the rat: Modulatory role of vitamin C, vitamin E and quercetin, Hum. Exp. Toxicol. 25 (5) (2006) 251–259, https://doi.org/10.1191/0960327106ht621oa.
[9] J.M. Simons, B.A. 't Hart, T.R.A.M. Ip Vai Ching, H. Van Dijk, R.P. Labadie, Metabolic activation of natural phenols into selective oxidative burst agonists by activated human neutrophils, Free Radic. Biol. Med. 8 (3) (1990) 251–258, https://doi.org/10.1016/0891-5849(90)90070-Y.
[10] S. Hougee, A. Hartog, A. Sanders, Y.M.F. Graus, M.A. Hoijer, J. Garssen, W.B. van den Berg, H.M. van Beuningen, H.F. Smit, Oral administration of the NADPH-oxidase inhibitor apocynin partially restores diminished cartilage proteoglycan synthesis and reduces inflammation in mice, Eur. J. Pharmacol. 531 (1-3) (2006) 264–269, https://doi.org/10.1016/j.ejphar.2005.11.061.
[11] A.A. Müller, S.A. Reiter, K.G. Heider, H. Wagner, Plant-derived acetophenones with antiasthmatic and anti-inflammatory properties: Inhibitory effects on chemotaxis, right angle light scatter and actin polymerization of polymorphonuclear granulocytes, Planta Med. 65 (1999) 590–594, https://doi.org/10.1055/s-1999-14029.
[12] R.B.R. Muijsers, E. Van Den Worm, G. Folkerts, C.J. Beukelman, A.S. Koster, D. S. Postma, F.P. Nijkamp, Apocynin inhibits peroxynitrite formation by murine macrophages, Br. J. Pharmacol. 130 (2000) 932–936, https://doi.org/10.1038/sj.bjp.0703401.
[13] F.P.J.G. Lafeber, C.J. Beukelman, E. Van Den Worm, J.L.A.M. Van Roy, M. E. Vianen, J.A.G. Van Roon, H. Van Dijk, J.W.J. Bijlsma, Apocynin, a plant-derived, cartilage-saving drug, might be useful in the treatment of rheumatoid arthritis, Rheumatology 38 (1999) 1088–1093, https://doi.org/10.1093/rheumatology/38.11.1088.
[14] Z. Guleken, P. Jakubczyk, P. Wiesław, P. Krzysztof, H. Bulut, E. Öten, J. Depciuch, N. Tarhan, Characterization of Covid-19 infected pregnant women sera using laboratory indexes, vibrational spectroscopy, and machine learning classifications, Talanta 237 (2022) 122916, https://doi.org/10.1016/j.talanta.2021.122916.
[15] J. Depciuch, M. Parlinska-Wojtan, K. Rahmi Serin, H. Bulut, E. Ulukaya, N. Tarhan, Z. Guleken, Differential of cholangiocarcinoma disease using Raman spectroscopy combined with multivariate analysis, Spectrochim. Acta - Part A Mol. Biomol. Spectrosc. 272 (2022) 121006, https://doi.org/10.1016/j.saa.2022.121006.
[16] Z. Guleken, B. Ünübol, R. Bilici, D. Sarıbal, S. Toraman, O. Gündüz, S. Erdem Kuruca, Investigation of the discrimination and characterization of blood serum structure in patients with opioid use disorder using IR spectroscopy and PCA-LDA analysis, J. Pharm. Biomed. Anal. 190 (2020) 113553.
[17] Z. Guleken, H. Bulut, G.İ. Gültekin, S. Arıkan, İ. Yaylım, M.T. Hakan, D. Sönmez, N. Tarhan, J. Depciuch, Assessment of structural protein expression by FTIR and biochemical assays as biomarkers of metabolites response in gastric and colon cancer, Talanta 231 (2021) 122353, https://doi.org/10.1016/j.talanta.2021.122353.
[18] Z. Guleken, Y. Tuyji Tok, P. Jakubczyk, W. Paja, K. Pancerz, Y. Shpotyuk, J. Cebulski, J. Depciuch, Development of novel spectroscopic and machine learning methods for the measurement of periodic changes in COVID-19 antibody level, Measurement 196 (2022) 111258.
[19] Z. Guleken, D. Ozbeyli, M. Acikel-Elmas, S. Oktay, B. Alev, S. Sirvanci, A. Velioglu Ogunc, O. Kasimay Cakir, The effect of estrogen receptor agonists on pancreaticobiliary duct ligation induced experimental acute pancreatitis., J. Physiol. Pharmacol. 68 (2017) 847–858. http://www.ncbi.nlm.nih.gov/pubmed/29550797 (accessed April 13, 2020).
[20] F.F. Jubaidi, R.D. Mathialagan, M.M. Noor, I.S. Taib, S.B. Budin, Monosodium glutamate daily oral supplementation: Study of its effects on male reproductive system on rat model, Syst. Biol. Reprod. Med. 65 (3) (2019) 194–204, https://doi.org/10.1080/19396368.2019.1573274.
[21] K.M. Köroğlu, Ö. Çevik, G. Şener, F. Ercan, Apocynin alleviates cisplatin-induced testicular cytotoxicity by regulating oxidative stress and apoptosis in rats, Andrologia 51 (4) (2019) e13227, https://doi.org/10.1111/and.13227.
[22] N.R.C. (US) C. for the U. of the G. for the C. and U. of L. Animals, Guide for the Care and Use of Laboratory Animals, Guid. Care Use Lab. Anim. (2011). https://doi.org/10.17226/12910.
[23] H. Ohkawa, N. Ohishi, K. Yagi, Assay for lipid peroxides in animal tissues by thiobarbituric acid reaction, Anal. Biochem. 95 (2) (1979) 351–358, https://doi.org/10.1016/0003-2697(79)90738-3.
[24] Y. Sun, L.W. Oberley, Y. Li, A simple method for clinical assay of superoxide dismutase, Clin. Chem. 34 (1988) 497–500, https://doi.org/10.1093/clinchem/34.3.497.
[25] E. BEUTLER, O. DURON, B.M. KELLY, Improved method for the determination of blood glutathione., J. Lab. Clin. Med. 61 (1963) 882–888. http://europepmc.org/article/med/13967893 (accessed March 12, 2022).
[26] B.W. Matthews, Comparison of the predicted and observed secondary structure of T4 phage lysozyme, BBA - Protein Struct. 405 (2) (1975) 442–451, https://doi.org/10.1016/0005-2795(75)90109-9.
[27] T. Fawcett, An introduction to ROC analysis, Pattern Recognit. Lett. 27 (8) (2006) 861–874, https://doi.org/10.1016/j.patrec.2005.10.010.
[28] L. Breiman, Random forests, Mach. Learn. 45 (2001) 5–32, https://doi.org/10.1023/A:1010933404324.
[29] S.L. Salzberg, C4.5: Programs for Machine Learning by J. Ross Quinlan. Morgan Kaufmann Publishers, Inc., 1993, Mach. Learn. 16 (1994) 235–240. https://doi.org/10.1007/bf00993309.
[30] N.S. Altman, An introduction to kernel and nearest-neighbor nonparametric regression, Am. Stat. 46 (3) (1992) 175–185, https://doi.org/10.1080/00031305.1992.10475879.
[31] Y. Goodfellow, I., Bengio, Y., Courville, A., Bengio, Deep Learning. The MIT Press, 2016. https://mitpress.mit.edu/books/deep-learning (accessed May 25, 2021).
[32] A. Zaknich, Statistical Learning Theory, Neural Networks Intell, Signal Process. (2003) 359–396, https://doi.org/10.1142/9789812796851_0014.
[33] T. Chen, C. Guestrin, XGBoost: A Scalable Tree Boosting System, in: Proc. 22nd ACM SIGKDD Int. Conf. Knowl. Discov. Data Min. (n.d.). https://doi.org/10.1145/2939672.
[34] Y. Ji, X. Yang, Z. Ji, L. Zhu, N. Ma, D. Chen, X. Jia, J. Tang, Y. Cao, DFT-Calculated IR spectrum Amide I, II, and III band contributions of N-methylacetamide fine components, ACS Omega 5 (15) (2020) 8572–8578, https://doi.org/10.1021/acsomega.9b0442110.1021/acsomega.9b04421.s001.
[35] M. Portaccio, S. Errico, T. Chioccarelli, G. Cobellis, M. Lepore, Fourier-Transform Infrared Microspectroscopy (FT-IR) Study on Caput and Cauda Mouse Spermatozoa, Proceedings 42 (2019) 19, https://doi.org/10.3390/ecsa-6-06537.
[36] M. Jackson, H.H. Mantsch, The use and misuse of FTIR spectroscopy in the determination of protein structure, Crit. Rev. Biochem. Mol. Biol. 30 (2) (1995) 95–120, https://doi.org/10.3109/10409239509085140.
[37] A. Barth, Infrared spectroscopy of proteins, Biochim. Biophys. Acta - Bioenerg. 1767 (9) (2007) 1073–1101, https://doi.org/10.1016/j.bbabio.2007.06.004.
[38] D.M. Byler, H. Susi, Examination of the secondary structure of proteins by deconvolved FTIR spectra, Biopolymers 25 (3) (1986) 469–487, https://doi.org/10.1002/bip.360250307.
[39] M. Pachetti, L. Zupin, I. Venturin, E. Mitri, R. Boscolo, F. D'amico, L. Vaccari, S. Crovella, G. Ricci, L. Pascolo, Ftir spectroscopy to reveal lipid and protein changes induced on sperm by capacitation: bases for an improvement of sample selection in art, Int. J. Mol. Sci. 21 (2020) 1–16, https://doi.org/10.3390/ijms21228659.
[40] C.G. Abdallah, L. Jiang, H.M. De Feyter, M. Fasula, J.H. Krystal, D.L. Rothman, G. F. Mason, G. Sanacora, Glutamate metabolism in major depressive disorder, Am. J. Psychiatry. 171 (12) (2014) 1320–1327, https://doi.org/10.1176/appi.ajp.2014.14010067.
[41] S. Zhu, E. Gouaux, Structure and symmetry inform gating principles of ionotropic glutamate receptors, Neuropharmacology 112 (2017) 11–15, https://doi.org/10.1016/j.neuropharm.2016.08.034.
[42] K. Niaz, E. Zaplatic, J. Spoor, Extensive use of monosodium glutamate: A threat to public health? EXCLI J. 17 (2018) 273–278, https://doi.org/10.17179/excli2018-1092.
[43] S.S. Barbieri, L. Sandrini, L. Musazzi, M. Popoli, A. Ieraci, Apocynin prevents anxiety-like behavior and histone deacetylases overexpression induced by sub-chronic stress in mice, Biomolecules 11 (6) (2021) 885, https://doi.org/10.3390/biom11060885.
[44] Z. Mustafa, S. Ashraf, S. Fareeha Tauheed, S. Ali, Monosodium Glutamate, Commercial Production, Positive and Negative Effects on Human Body and Remedies-A Review, 4 (2017) 425–435. www.ijsrst.com (accessed March 12, 2022).
[45] J. Choi, G.J. Im, J. Chang, S.W. Chae, S.H. Lee, S.-Y. Kwon, A.-Y. Chung, H.-C. Park, H.H. Jung, Protective effects of apocynin on cisplatin-induced ototoxicity in an auditory cell line and in zebrafish, J. Appl. Toxicol. 33 (2) (2013) 125–133, https://doi.org/10.1002/jat.1729.
[46] Q.Z. Chen, W.Q. Han, J. Chen, D.L. Zhu, C.Y. Chen-Yan, P.J. Gao, Anti-stiffness effect of apocynin in deoxycorticosterone acetate-salt hypertensive rats via inhibition of oxidative stress, Hypertens. Res. 36 (2013) 306–312, https://doi.org/10.1038/hr.2012.170.
[47] C.M. Rosa, R. Gimenes, D.H.S. Campos, G.N. Guirado, C. Gimenes, A.A. H. Fernandes, A.C. Cicogna, R.M. Queiroz, I. Falcão-Pires, D. Miranda-Silva, P. Rodrigues, F.R. Laurindo, D.C. Fernandes, C.R. Correa, M.P. Okoshi, K. Okoshi, Apocynin influence on oxidative stress and cardiac remodeling of spontaneously hypertensive rats with diabetes mellitus, Cardiovasc. Diabetol. 15 (1) (2016), https://doi.org/10.1186/s12933-016-0442-1.